Clim Dyn (2009) 32:313–332
DOI 10.1007/s00382-008-0464-9

Aerosol direct forcing of the summer Indian monsoon as simulated by the NCAR CAM3

J. Craig Collier · Guang J. Zhang

Received: 15 August 2007 / Accepted: 18 August 2008 / Published online: 14 October 2008
© Springer-Verlag 2008

Abstract In this study, the effects of aerosols on the simulation of the Indian monsoon by the NCAR Community Atmosphere Model CAM3 are measured and investigated. Monthly mean 3D mass concentrations of soil dust, black and organic carbons, sulfate, and sea salt, as output from the GOCART model, are interpolated to mid-month values and to the horizontal and vertical grids of CAM3. With these mid-month aerosol concentrations, CAM3 is run for a period of approximately 16 months, allowing for one complete episode of the Indian monsoon. Responses to the aerosols are measured by comparing the mean of an ensemble of aerosol-induced monsoon simulations to the mean of an ensemble of CAM3 simulations in which aerosols are omitted, following the method of Lau et al. (2006) in their experiment with the NASA finite volume general circulation model. Additionally, an ensemble of simulations of CAM3 using climatological mid-month aerosol concentrations from the MATCH model is composed for comparison. Results of this experiment indicate that the inclusion of aerosols results in drops in surface temperature and increases in precipitation over central India during the pre-monsoon months of March, April, and May. The presence of aerosols induces tropospheric shortwave heating over central India, which destabilizes the atmosphere for enhanced convection and precipitation. Reduced shortwave heating and enhanced evaporation at the surface during April and May results in reduced terrestrial emission to cool the lower troposphere, relative to simulations with no aerosols. This effect weakens the near-surface cyclonic circulation and, consequently, has a negative feedback on precipitation during the active monsoon months of June and July.

Keywords Indian monsoon · Climate model · Direct effect

J. C. Collier (✉) · G. J. Zhang
Center for Atmospheric Sciences, Scripps Institution of Oceanography, 9500 Gilman Drive, Dept. 0221, La Jolla, CA 92093-0221, USA
e-mail: craigc@fiji.ucsd.edu; craig.collier@garradhassan.com

1 Introduction

The forcing of the climate system by the radiative effects of aerosols has received considerable research attention over the past several years. Given the uncertainties in their concentration and size distribution estimates, the large variability in their geographic distribution, and the complex nature of their interactions with clouds at various levels in the atmosphere, aerosols, and specifically quantification of their forcing on the climate system, remain a challenging complication in the estimation and prediction of climate change. Notwithstanding, anthropogenic aerosol loadings have increased since preindustrial times and continue to increase around and downwind of global industrial centers as well as rural regions plagued by biomass burning. Studies of the effects of these increased loadings on the architecture of the climate system will continue for years to come.

Detailed analyses of the effects of aerosols on radiation in the atmosphere date back to at least the 1970s. In 1972, Neumann and Cohen (1972) used a simple model to show that placement of a single layer of aerosols near the surface of the Earth generally induces a loss of energy to the earth-atmosphere system (the direct effect), while placing a layer near the surface and one in the upper atmosphere can, if absorption is sufficiently large and backscatter is not too large, actually lead to a net gain. But effects are

highly-species dependent. For example, organic carbons and sulfates are important for radiative scattering (Charlson et al. 1992; Kiehl and Briegleb 1993; Boucher and Anderson 1995); dust and black carbon, on the other hand, can be effective radiative absorbers (Andreae 2001; Satheesh and Srinivasan 2002; Kim et al. 2006; Satheesh et al. 2007; Moorthy et al. 2007). The presence of clouds vertically stratifies the heating effects. For example, stratus cloud at 3–4 km in the presence of aerosols results in enhancement of heating above the cloud and a reduction of heating immediately below it (Braslau and Dave 1975). However, effects such as these depend on cloud thickness as well (Liao and Seinfeld 1998). Other effects on aerosol top-of-atmosphere (TOA) radiative forcing include internal and external mixing of certain species with other species (Liao and Seinfeld 1998), whether the aerosols absorb water (Charlock and Sellers 1980), the ambient atmospheric conditions, and where the aerosols are located with respect to the Sun (Nemesure et al. 1995).

In the twenty-first century, there has been a growing number of important aerosol forcing-related field campaigns, particularly over the northern Indian Ocean, a region plagued by the well-known Indo-Asian haze (Ramanathan et al. 2001a). This phenomenon is an especially important problem given the large south Asian population and the region's potential for growing pollutant emissions (Lelieveld et al. 1993). From the Indian Ocean Experiment (INDOEX) campaign, Ramanathan et al. (2001b) found that the human-produced contribution to aerosols over this area weighed in at about 80%, with soot, via radiative absorption, contributing significantly to the total atmospheric forcing. Furthermore, they showed that surface forcing can impact the hydrologic cycle and potentially the thermohaline circulation due to its cooling effect on the Indian Ocean. The study is joined by a number of other investigations also focused on this region of the world (Li and Ramanathan 2002; Collins et al. 2002; Babu et al. 2004; Moorthy et al. 2005; Ramana and Ramanathan 2006; Corrigan et al. 2006) which document the interannual, seasonal, diurnal, and geographic variability of aerosol forcing.

In recent years, state-of-the-art general circulation models have been used to simulate aerosol effects on climate relative to greenhouse gas warming (Takemura et al. 2002, 2005; Kristjansson et al. 2005) as well as effects on precipitation and atmospheric convective instability (Chung and Zhang 2004). Two recent model experiments which focused on aerosol forcing for south Asian climate have shown interesting results. In 2002, Menon et al. (2002b) applied incremental aerosol optical depths to the Goddard Institute for Space Studies (GISS) S12000 12-layer climate model for 120-year simulations over India and China. They found that black carbon, via tropospheric heating, increases local convection, precipitation, and surface cooling over these regions and thereby modifies large-scale circulation. In 2006, Lau et al. (2006) forced the National Aeronautics and Space Administration (NASA) finite volume general circulation model with aerosol optical depths (AODs) as output by the Georgia Institute for Technology - Goddard Global Ozone Chemistry Aerosol Radiation and Transport Model (GOCART), to measure the direct radiative forcing of aerosols on the Asian summer monsoon. GOCART is a 3D aerosol model driven by assimilated meteorological fields. One of the primary findings of their sensitivity studies is that heating of the air by dust and black carbon on the slopes of the Tibetan Plateau forces dry convection, a so-called "elevated heat pump" during March-April, and triggers a moist convective feedback via the so-called elevated-heat-pump effect, advancing the rainy season, and intensifying the monsoon rain in May–June–July Lau and Kim (2006). Most recently, an increase in pre-monsoonal rainfall due to black carbon, was observed in simulations of the community climate system model version 3 by Meehl et al. (2008). The latest version of the NCAR model, the community atmosphere model (CAM3), allows input of time-varying three-dimensional aerosol mass distribution, a significant advancement over its predecessor. The current study takes advantage of this functionality and examines the aerosol forcing on the Indian monsoon simulated by CAM3. Furthermore, as in previous studies, it attempts to explain the physical causes of any aerosol-induced effects produced.

2 Models

2.1 NCAR community atmosphere model (CAM3)

The model used for simulating both the transport and the direct radiative effects of aerosols is the National Center for Atmospheric Research (NCAR) Community Atmosphere Model, ver. 3 (CAM3) (Collins et al. 2004). This serves as the atmospheric component of the Community Climate System Model, ver. 3 (CCSM3) (Collins et al. 2006), and is coupled to the Community Land Surface Model, ver. 3 (CLM3) described in Oleson and coauthors (2004) and Dickinson et al. (2006). In fully coupled mode, the atmospheric model interfaces with an ocean model; however, for this project, the oceanic conditions were communicated to the atmosphere via an oceanic surface boundary condition, given as mid-month values of sea-surface temperature (SST) interpolated to the model's grid and provided by the Program for Climate Model Diagnosis and Intercomparison (PCMDI) at Lawrence Livermore National Laboratory (LLNL) (Taylor et al. 2000). For this study, it operates at T42 horizontal resolution, which

prescribes a roughly uniform 2.8° × 2.8° Gaussian grid on the Earth's surface. Vertically, the model evaluates three-dimensional atmospheric variables on 26 levels, where lowest levels are given in sigma coordinates and uppermost levels are specified in pure pressure coordinates. While the model incorporates a variety of physical parameterizations, the one most important for the current study is that for deep convection. Deep convection is given by the scheme of Zhang and McFarlane (1995), which characterizes the subgrid-scale vertical transport of heat and moisture by ensembles of entraining plumes. The scheme is closed by determination of convective available potential energy (CAPE), which is consumed exponentially at a characteristic time scale.

In its present configuration, the 3D time-dependent distributions of five aerosol species and the optical parameters of each species are loaded into CAM3 upon initialization. These species are sea salt, sulfate, soil dust, and black and organic carbons, the latter three of which strongly absorb visible light. In addition, black and organic carbon can be either hydrophobic or hydrophilic. The relative humidity used to compute hygroscopic growth is 80%. The optical parameters defined for each of the aerosol types are specific extinction, single-scatter albedo, and the asymmetry parameter, and these are combined for each species into a single set of extinctions, albedoes, and asymmetry parameters for each layer. Optics for black and organic carbon follow from the optical properties of aerosols and clouds (OPAC) dataset (Hess et al. 1998), while those for dust are derived from Mie calculations for the size distribution associated with each size bin (Zender et al. 2003). Mid-month values of the mass paths of the aerosol species are interpolated to the current time step upon the model's integration. These are provided by a climatology file which is annually cyclic or can be specified by the user as implemented here (Collins et al. 2004).

2.2 GOCART model

Mid-month values of the mass paths of aerosol species were derived from output of the Georgia Institute of Technology—Goddard global ozone chemistry aerosol radiation and transport (GOCART) model. This model simulates all the major tropospheric aerosol types and runs at a horizontal resolution of 2° latitude by 2.5° longitude with 20–30 vertical sigma levels. It uses assimilated meteorological fields from the Goddard earth observing system data assimilation system (GEOS DAS), including such fields as winds, temperature, pressure, and specific humidity. The model is described in detail by Chin et al. (2002). The GOCART mass concentrations, specified in units of mass per volume at each grid point and each level were interpolated to the horizontal and vertical grids of CAM3. For some aerosol species, such as soil dust, the CAM3 and GOCART optical parameters are dependent on particle diameter and thus pertain to particular size distribution bins. Since some of the bins do not map uniformly between the two models, these mass concentrations have to be further interpolated from the GOCART bins to the CAM3 bins. However, this is not true for every aerosol species or for all bins of any particular species. Finally, for each level interface, the mass concentrations were numerically integrated from the surface upward to provide the aerosol path in units of mass per area at each level. This method of providing aerosol data to the GCM differs somewhat from that of Lau et al. (2006). In their experiment, aerosol optical depths (AODs) were provided to the NASA GCM. For the current study, the AODs were calculated by the CAM3 using the provided mass paths and internally-defined optical parameters of specific extinction, single scattering albedo, and asymmetry parameter, which give both black carbon and dust highly absorptive features for warming the atmosphere. Both dust and black carbon are well known to counterbalance cooling effects due to anthropogenic reflective aerosols like sea salt and sulfate; black carbon, in particular, may contribute significantly to the effects of carbon dioxide in global warming. The thermal effects of dust are less straightforward and highly dependent on vertical distribution. For example, dust in the stratosphere generally contributes to surface cooling by reflecting incoming solar radiation, while dust in the lower troposphere can contribute to surface warming by absorption of solar radiation and outgoing longwave radiation from the surface. The ranges of specific extinction (m^2g^{-1}), asymmetry parameter, and single scattering albedo for the most radiatively important aerosols are listed in Table 1 below.

2.3 CAM3 simulations

The simulations carried out for this experiment are modeled after those carried out for the Lau et al. (2006) experiment. To estimate the sensitivity of the monsoon simulation to the presence of tropospheric aerosols, differences were measured between an ensemble of CAM3 simulations using the monthly GOCART-derived aerosol mass paths, whose generation is described previously, and an ensemble of eight CAM3 simulations wherein the aerosol mass paths are always zero (no aerosols).[1] The latter set of simulations is forced by the same ozone mixing ratio and mid-month observed SSTs as the all-aerosol simulation. Since CAM3 also provides a standard

[1] Note that each member of an ensemble is initialized with a randomly-perturbed three-dimensional temperature field, which ensures the generation of unique climate states.

Table 1 Ranges of CAM3 optical parameters of extinction coefficient (m^2 g^{-1}), asymmetry parameter, and single-scattering albedo for soot, dust, sea salt, and sulfate

	Ranges of optical parameters					
	EXT		ASYM		SSA	
	Minimum	Maximum	Minimum	Maximum	Minimum	Maximum
Soot	0.87	23.48	0.04	0.53	0.003	0.31
Dust	0.02	2.85	0.07	0.95	0.53	0.98
Sea salt	0.24	6.17	0.71	0.93	0.68	1
Sulfate	0.05	110.11	0.267	0.8	0.41	1

file for aerosol loading, sensitivity to grid box differences in aerosol loading is estimated by carrying out simulations using the CAM3 climatological mid-month 3D mass concentrations. These concentrations are derived from the model for atmospheric transport and chemistry (MATCH), which was developed at NCAR and Scripps Institution of Oceanography. As this paper will show, the aerosol loadings from GOCART and from the climatology differ considerably for certain regions. Sensitivity of the regional-mean precipitation is measured with respect to the natural variability of the model, estimated by the 95% confidence interval on the ensemble mean monthly mean precipitation rate. All simulations begin on September 1, 2000 and continue through mid-2002, the length for which GOCART data is provided, allowing for evaluation of one complete annual cycle.

3 Results

3.1 Direct effects on surface climate

In the annual average, inclusion of aerosols into CAM3 results in widespread surface cooling. Although ocean temperatures are constrained by the SST boundary condition applied to the model, the simulated global average terrestrial surface temperature change for 2001 is about 0.15 K (not shown). Maps of the monthly mean surface temperature differences between the CAM3 GOCART all-aerosols run [hereafter referred to as CAM3 (GOCART)] and the CAM3 no-aerosols run [hereafter referred to as CAM3(NA)], are shown in Fig. 1 for the domain encompassing much of south-central Asia. These maps reveal that inclusion of aerosols in the CAM3 yields a cooling effect for the surface of central India, which expands in coverage and intensifies from March to May. For some locations in May, surface temperature is as much as 5 K lower than that simulated with no aerosols, and this is statistically significant at the 95% level. Similar cooling effect was found due to black carbon in the coupled model simulation by Meehl et al. (2008).

Prior to and upon monsoon onset, precipitation shows dramatic changes as well. As Fig. 2 shows, over central India, monthly mean precipitation differences are large and positive, particularly in May, with statistically-significant increases on the order of 1–2 mm day^{-1} in some locations. Patterns of precipitation increase to some extent resemble those of surface temperature decrease, and this is not a coincidence. Changes in cloud amount, associated with changes in rainfall, can strongly limit the rate of surface heating.

Over land, aerosol-induced changes in surface temperature and precipitation noticeably influence the simulated surface energy budget. We focus on the region of central India (outlined in Fig. 2), as this appears to be the area of greatest influence. It should be noted that this region of analysis is much smaller than the one considered in the Lau et al. (2006) experiment, of which it is a subset. However, as evident in Fig. 2, our region of comparison is comprised of very little ocean surface, whose temperature does not vary amongst the simulations anyway. Here we adopt the following formula for net change in surface energy:

$$\Delta E \approx \Delta \mathrm{SW} - \Delta \mathrm{LW} - \Delta \mathrm{SH} - \Delta \mathrm{LH}, \quad (1)$$

where SW and LW are shortwave heating and longwave cooling of the surface, respectively, and SH and LH are sensible and latent heat fluxes from the surface to the atmosphere.[2] The sign conventions are such that the net longwave flux, sensible and latent heat fluxes are positive upward. Thus a negative sign is added in front of the last three terms in Eq. 1. Refer to Table 2, which shows the values of these budget terms for April, May, June and July. Note that because of the sign convention in Eq. 1, in Table 1 a positive value for SW and δE means the surface gains more energy, and a positive value in LW, SH or LH means the surface loses more energy. During April, shortwave gain by the surface drops by 27 W m^{-2} while net longwave emission from the surface decreases by 14.2 W m^{-2}. These changes reflect an increase in the

[2] The equality is not exact since we are omitting changes due to ground energy storage, assumed to be effectively small.

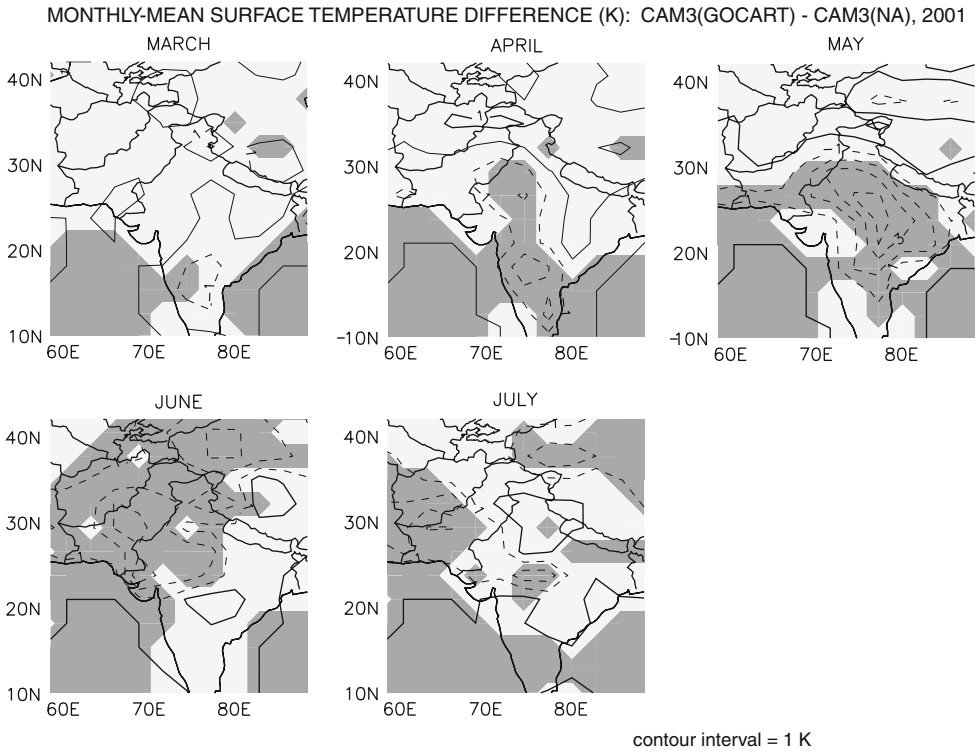

Fig. 1 Monthly-mean surface temperature difference (K) between the CAM3 (GOCART) and CAM3 (NA) runs for 2001. The contour interval is 1 K. Note that anomalies significant at the 95% level are shaded in *gray*

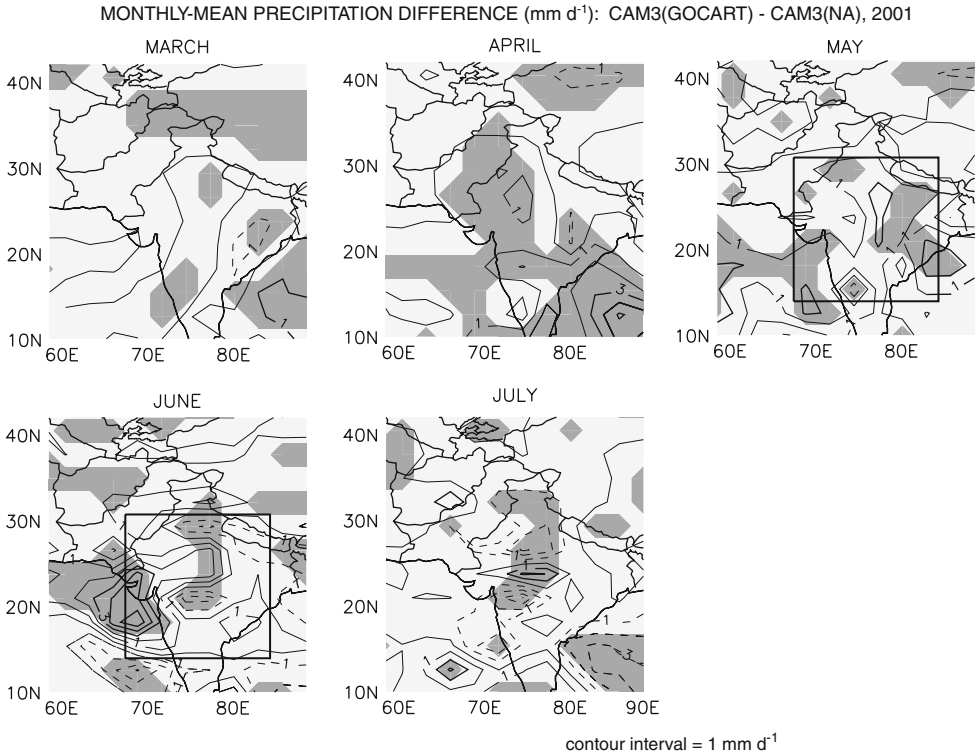

Fig. 2 Monthly-mean precipitation difference (mm day^{-1}) between the CAM3 (GOCART) and CAM3 (NA) runs for 2001. The *box* represents the central India region (73–84°E, 15–27°N). Contour interval is 1 mm day^{-1}. Note that anomalies significant at the 95% level are shaded in *gray*

amount of cloud cover. Downwelling solar radiation is scattered by the tops of the clouds, thereby reducing the amount of shortwave energy to the surface. Reduced surface temperature together with the cloud greenhouse effect decreases the surface longwave flux. The sensible heat flux into the overlying atmosphere also decreases due to colder surface temperature. However, as will be shown in the next section, the presence of absorptive aerosols increases

Table 2 Aerosol-induced changes in surface shortwave heating (SW), longwave heating (LW), sensible heat flux (SH), and latent heat flux (LH) as averaged over the Central India region for the months of April, May, and June, 2001

Surface energy changes (W m^{-2})					
Month	SW	LW	SH	LH	ΔE
April	−27.0	−14.2	−13.3	+2.6	**−2.1**
May	−25.1	−16.0	−15.3	+8.6	**−2.4**
June	−27.0	−8.3	−8.5	−4.2	**−6.0**
July	−7.3	1.3	−4.4	−6.0	**+1.8**

atmospheric absorption of solar energy, which warms the atmosphere. It is speculated that the latent heat flux to the atmosphere increases due to increased rainfall, which increases the soil moisture. However, it is also possible that strong winds associated with the convection may also impart an increase in latent flux as well. Relative to those for April, the radiative changes in May and June are similar. Shortwave heating drops by 25–27 W m^{-2}, and longwave emission is reduced, though less so in June. Meanwhile, strong surface cooling is reflected by the large drop in sensible heat flux, while increased rainfall in May, and thus increased surface humidity, is reflected by the increase in latent heat flux. Note that there is a decrease in the latent heat flux for June. This trend can be attributed to the areas for which precipitation decreases. Note from Fig. 2 that, in addition to the wet area over central India and the northwestern Arabian Sea, there is a large region of drying over the eastern part of the country, extending into the Bay of Bengal. By July, this region of reduced rainfall is expanded over nearly all of the subcontinent. This will be discussed in more detail later. Overall, for central India (73°E–84°E; 15°N–27°N), the effect of aerosols on surface energy budget during the pre-monsoon phase (April) and the mature phase of the simulated monsoon (May–June) is a removal of energy from the surface due to enhanced evaporation (LH) (except June) and reduced insolation (SW), which are offset by reductions in longwave and sensible loss. For July, the reduced solar flux is overcompensated by reduced surface sensible and latent heat fluxes, resulting in a small gain in energy.

3.2 Sensitivity to aerosol loading

To estimate the sensitivity of the above-described effects on surface climate to geographic aerosol loading pattern, a parallel set of simulations using the MATCH-derived climatological aerosol mass distributions also was carried out. Indeed, there are some remarkable differences between the aerosol loading patterns of the GOCART and MATCH-derived distributions. These differences are depicted in Fig. 3. When integrated from the top model level to the surface, April–July dust in the GOCART run is substantially more concentrated than in the MATCH run just north of the Himalayas, or on the northern slope of the Tibetan Plateau. In fact, relative to the MATCH data, the GOCART data shows 20 times as much dust over this region. The MATCH data appears to be lacking a significant dust source over the Takla Makhan desert of western China. Meanwhile, relative to the MATCH run, both dust and black carbon are underrepresented in the GOCART run over India, where the concentrations are between 40 and 60% less than those from MATCH. At these latitudes, much of the dust over India is transported by southwesterly winds from the Arabian peninsula, while significant amounts of black carbon, emanating from pollution sources on the Indo-Gangetic Plain (Lau and Kim 2006) appear most concentrated over extreme eastern India, at the northern end of the Bay of Bengal.

3.2.1 Effects on simulated shortwave heating

As shown by Lau et al. (2006) for the NASA model, the presence of aerosols can contribute significantly to atmospheric shortwave heating. Over the high-albedo Tibetan Plateau, they found strong simulated effective absorption from multiple reflections between an aerosol layer and the land surface. Aerosol-induced heating occurs in the NCAR model as well, as shown in the zonal mean relative atmospheric shortwave heating anomaly, as averaged over the central India longitudes (70–84°E) in Fig. 4a. Relative to the no-aerosols realizations, both the MATCH and GOCART runs show a 5–10% increase in atmospheric shortwave heating over the latitudes of India (10°–30°N), increasing with elevation on the Tibetan Plateau. While the MATCH runs show somewhat greater heating above the southern slope of the plateau (27°–30°N), the GOCART runs exhibit considerably greater heating over the northern slope, exceeding the shortwave heating of the no-aerosols simulations by greater than 40%. The heating anomaly is a direct function of the concentration of absorptive aerosols like dust and black carbon, whose zonal-mean concentrations are shown in Fig. 4b–c. The GOCART data provides greater dust and black carbon on the northern slope latitudes, while the MATCH data provides greater concentrations to the south, consistent with the loading differences maps in Fig. 3.

3.2.2 Effects on simulated precipitation

Interestingly, the precipitation anomalies of central India, as discussed in the previous section, are relatively similar regardless of which aerosol data is used. This is

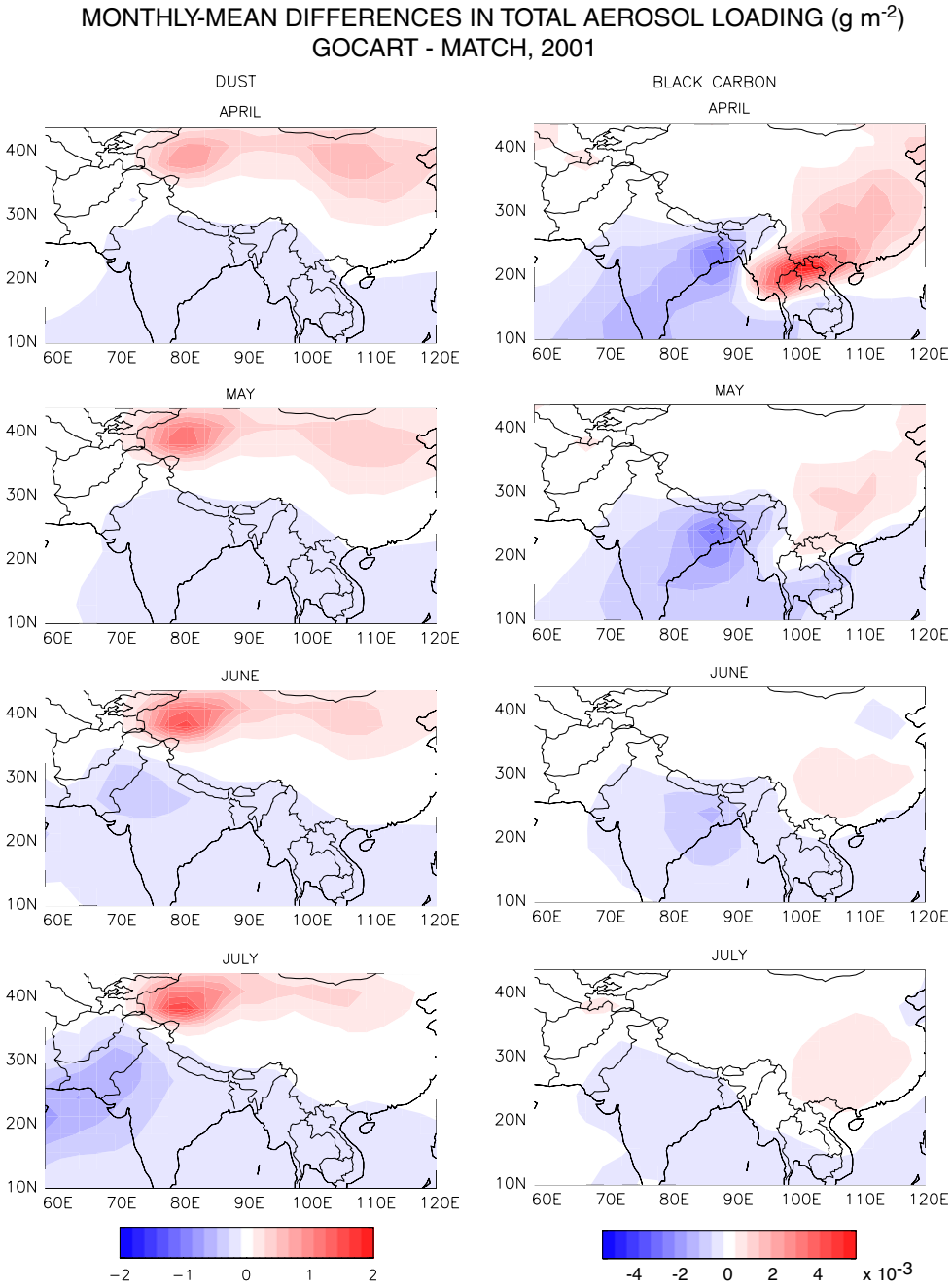

Fig. 3 Monthly-mean differences in aerosol mass concentration for 2001, as integrated from the *top* CAM3 model layer to the surface, between the CAM3 (GOCART) and CAM3 (MATCH) runs. Note the difference in scale between the dust and black carbon differences

exemplified by Fig. 5, which shows the monthly-mean precipitation rates, averaged over the region, as simulated by the MATCH and GOCART runs of the model and as observed in the Xie–Arkin data for 2001. Note the model's considerable wet bias relative to the observations. With aerosols or not, the model simulates nearly twice as much rain as observed annually for this region. Any observational uncertainty likely is small, since the annual mean rainfall calculated from observations of NASA's tropical rainfall measuring mission (TRMM) satellite (not shown) is only about 6% lower than that calculated from the Xie-Arkin data. However, in spite of the model's bias, a strong monsoon signal is present, both in the simulations and in the observations. The inclusion of aerosols significantly enhances through March, April, and May and by as much as 15% during June, though this increase is not quite significant at the 95% level. However, it is important to point out that increases in smaller subregions within the large averaging domain are more significant, particularly over east-central India in May and along the

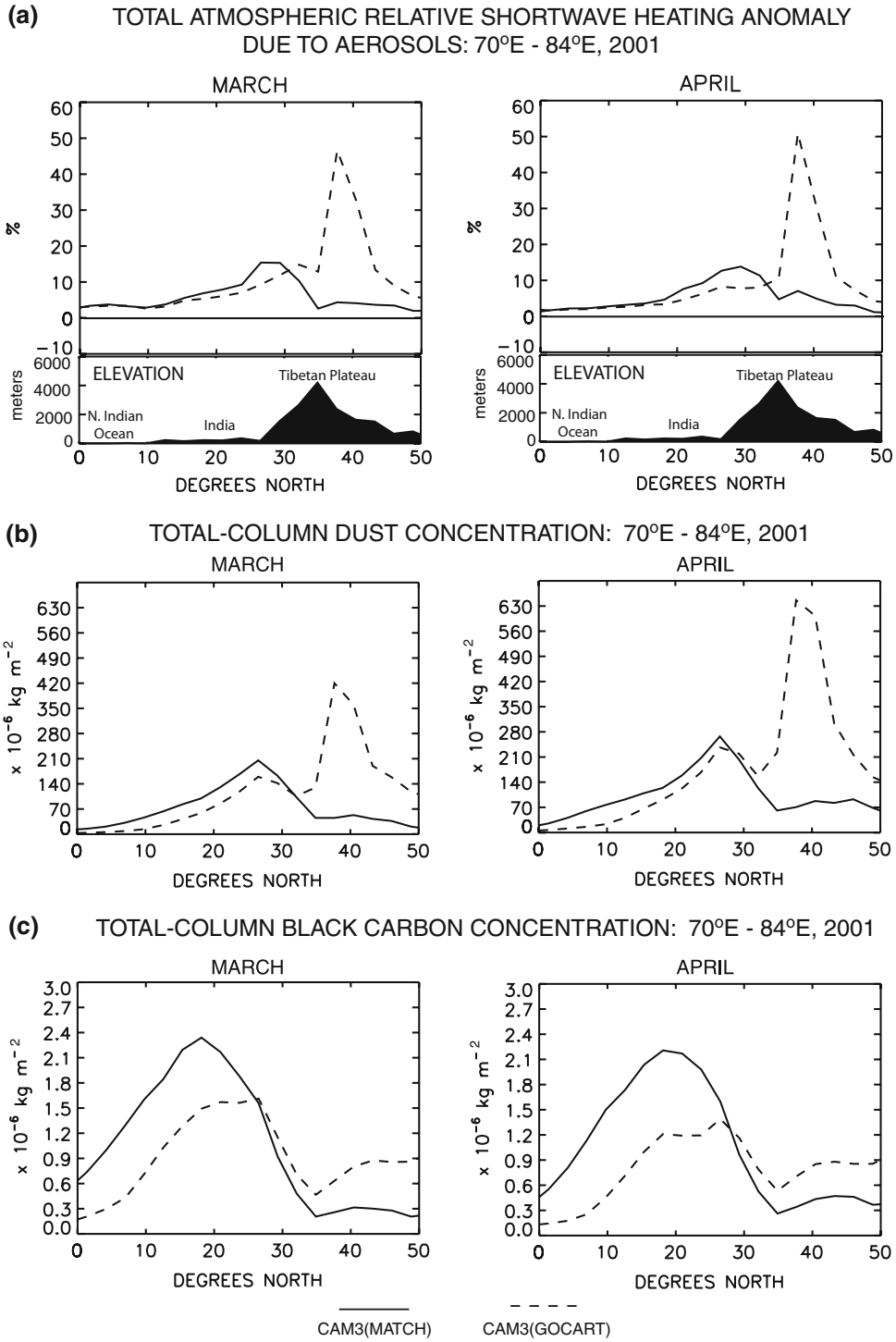

Fig. 4 Total atmospheric relative shortwave heating anomaly due to aerosols (%) (**a**) and total-column dust and black carbon concentrations (kg m^{-2}; **b** and **c**, respectively) for March and April, 2001 from the CAM3 (MATCH) and CAM3 (GOCART) simulations as averaged over the central India region for latitudes between the Equator and 50°N

western coast of India in June (see Fig. 2). This may be a key difference between the results obtained here and those obtained by Lau et al. (2006); here the effects may be more geographically isolated. There are other notable differences between these results and those obtained by Lau et al. (2006). While the NASA model showed an increase for July precipitation, upon inclusion of aerosols, the NCAR model shows a sharp decrease this month, as also seen from the contour map for July shown in Fig. 2. In fact, the aerosol-forced runs show an annual precipitation peak in June, one month earlier than the peak from the observations and that from the unforced runs. This feature is produced regardless of which aerosol distribution is used. The same qualitative features are obtained by

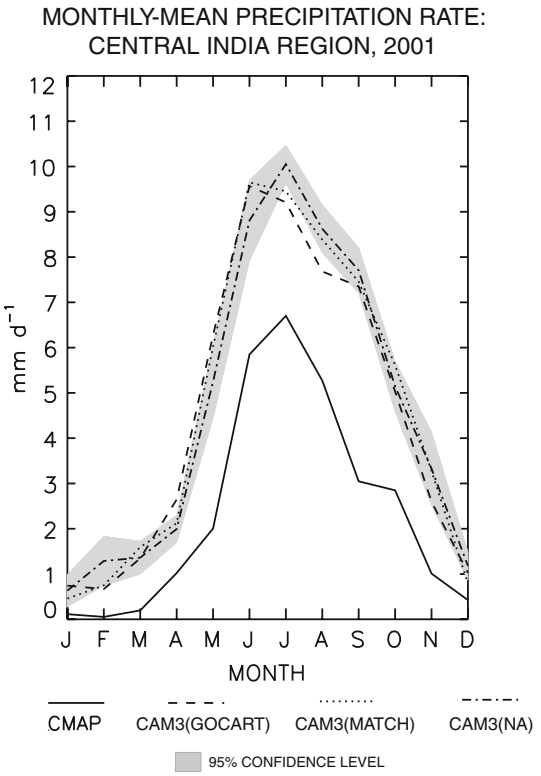

Fig. 5 Monthly-mean precipitation as averaged over the central India region for CAM3 simulations with GOCART aerosols (*dashed*), climatological MATCH aerosols (*dotted*), and no aerosols (*dash-dotted*), as well as for Xie–Arkin monthly precipitation data (*solid*). The *light gray shading* represents the 95% confidence level on statistical significance of a difference from the ensemble mean of the no-aerosols simulations

Meehl et al. (2008) in their coupled model simulation using the NCAR CCSM3 to investigate the effect of black carbon. They noted that including black carbon in the CCSM3 enhances pre-monsoon (March–May) precipitation and reduces monsoon season precipitation (June–August).

3.2.3 Species-dependent effects

In order to isolate the effects of individual aerosol species, additional simulation ensembles were composed in which either dust or black carbon were omitted from the aerosol loading. Anomalies due to black carbon were estimated by subtracting those due to all species except black carbon from those due to all species. A similar calculation was performed for dust. Seasonal-mean precipitation anomalies are contoured in Fig. 6. During the pre-monsoon months of MAM, it is evident that black carbon contributes more significantly to precipitation increases over the continent, particularly over northern India and the Tibetan Plateau. Dust contributes to increases further south, particularly in the western Bay of Bengal. For the most part, both dust and black carbon contribute to decreases in precipitation during the monsoon months of JJA, though dust contributes to isolated regions of increased precipitation in central India. Such results are not inconsistent with those of the Meehl et al. (2008) study, which shows black carbon-induced increased precipitation in the pre-monsoon months over northern India and decreased precipitation due to black carbon during JJA. However, it is worth noting an important difference in that for the simulations described herein, SST is not allowed to be sensitive to changes in aerosol concentration. Therefore, decreased precipitation during JJA cannot be the result of a black carbon-induced weakening of the latitudinal SST gradient.

3.2.4 Vertical and meridional anomalies

The evolution of the simulated monsoon is investigated more thoroughly by evaluation of the vertical distribution of temperature and circulation anomalies, as induced by the presence of aerosols. The monthly-mean vertical distribution of temperature, meridional circulation, precipitation, heating, and cloud anomalies are shown for the MATCH and GOCART runs in Figs. 7 and 8, respectively. Note that precipitation anomalies are stratified by stable condensation, shallow convective, and deep convective and that cloud fraction anomalies are contoured on top of those for condensational heating, with which they are well correlated. These figures reveal the dramatic effect of absorbing aerosols on simulated atmospheric heating and hydrology. Both sets of simulations show similar monthly mean temperature anomalies, with strong warming above the southern slope in March, concurrent with enhanced upward motion from the surface. Much of the heating is due to enhanced shortwave absorption, as shown in the shortwave heating anomaly. The weakly enhanced longwave heating likely is due to downward emission from increased cloud at 200–300 hPa. Cooling near the surface begins in earnest during the month of April with a well-defined anomalous meridional circulation characterized by large-scale ascent over the southern slope and large-scale descent over the northern slope and the northern Indian Ocean. While this appears at least a month too early, relative to the experiment by Lau et al. (2006), it is the manifestation of the "elevated heat pump", so described by their study and the observational study of Lau and Kim (2006). Via shortwave absorption, absorptive aerosols like dust and black carbon heat the atmosphere, causing air to rise. To fill the void, moisture-laden air is drawn in from the Indian Ocean, as represented by the slightly poleward-component of the circulation at mid-levels this month. The moisture condenses, forming clouds, and thus precipitation. Rainfall is

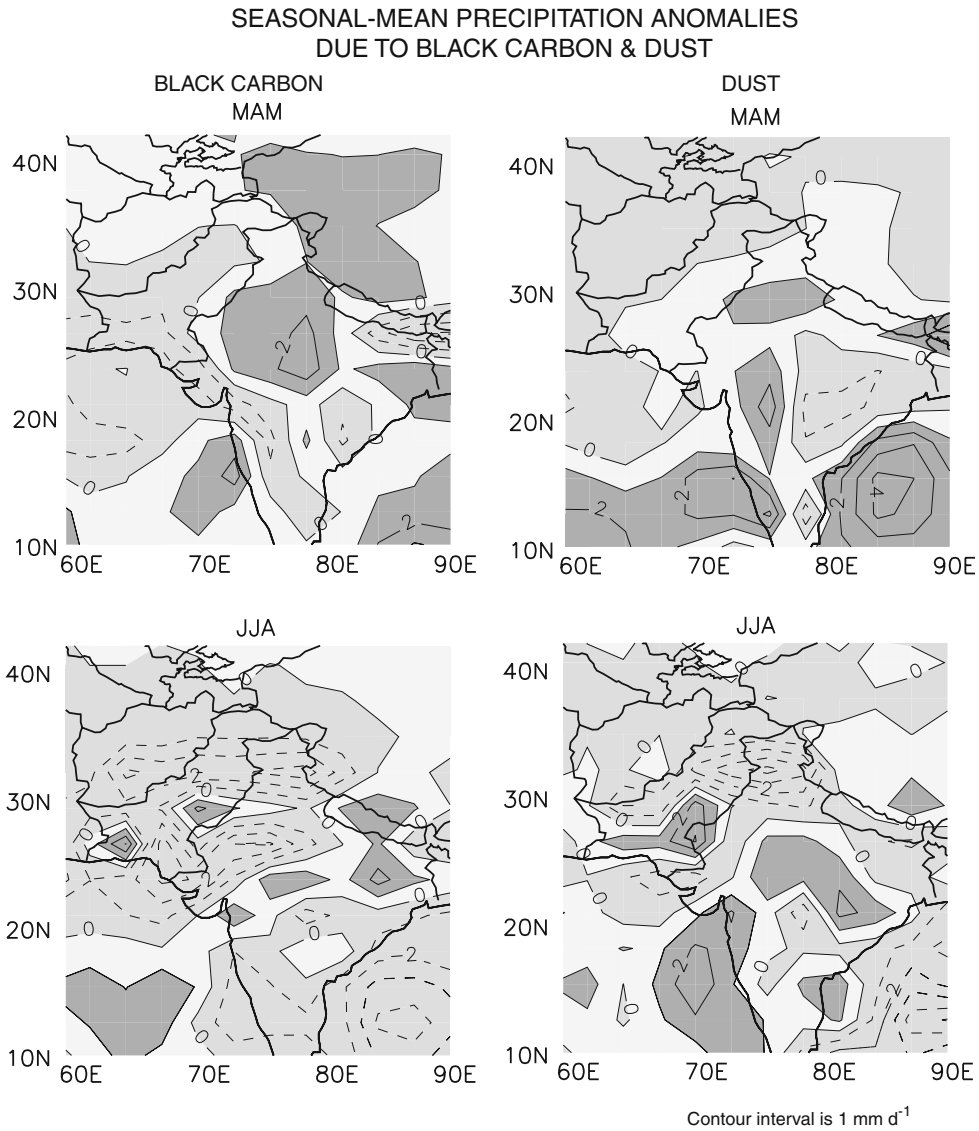

Fig. 6 Seasonal-mean precipitation anomaly for 2001, due to black carbon (*left*) and due to dust (*right*). Note that reduced precipitation is indicated by *light gray shading* while increased precipitation is indicated by *dark gray shading*

reduced under the branches of descent associated with this circulation anomaly.

As the monsoon strengthens, the positive cloud anomaly is expanded northward during May. Cooling at the surface is a reflection of this cloud anomaly, as clouds effectively reduce the amount of shortwave energy to the Earth's surface, thereby reducing the release of terrestrial radiation to warm the overlying atmosphere. This effect is demonstrated well by comparison between the longwave heating and temperature anomalies over lower India and the Himalayan foothills (10°–30°N). Reduction of vertical heat diffusion by turbulent processes contributes significantly to the cooling as well (not shown). Over the higher elevation slopes, the enhanced near-surface shortwave heating actually can cancel atmospheric cooling due to reduced vertical diffusion and reduced terrestrial emission. This is particularly apparent on the northern slope of the plateau for both sets of runs during March–May and can be attributed to a higher surface albedo and increased particulate loading relative to surrounding latitudes (recall Fig. 4). Also during May, the near-surface cooling on the southern slope reaches a maximum of nearly 3 K relative to simulations with no aerosols, and cloud has increased over the depth of the troposphere from roughly 15–30°N. Consistent with the increased cloud, precipitation resulting from deep convection is significantly increased over much of India by nearly 1 mm day^{-1} in the MATCH runs and by nearly 1.25 mm day^{-1} in the GOCART runs.

In June, enhanced near-surface latent heating, combined with the existing shortwave heating reduces the overall cool anomaly on the southern slope, and just as in the Lau

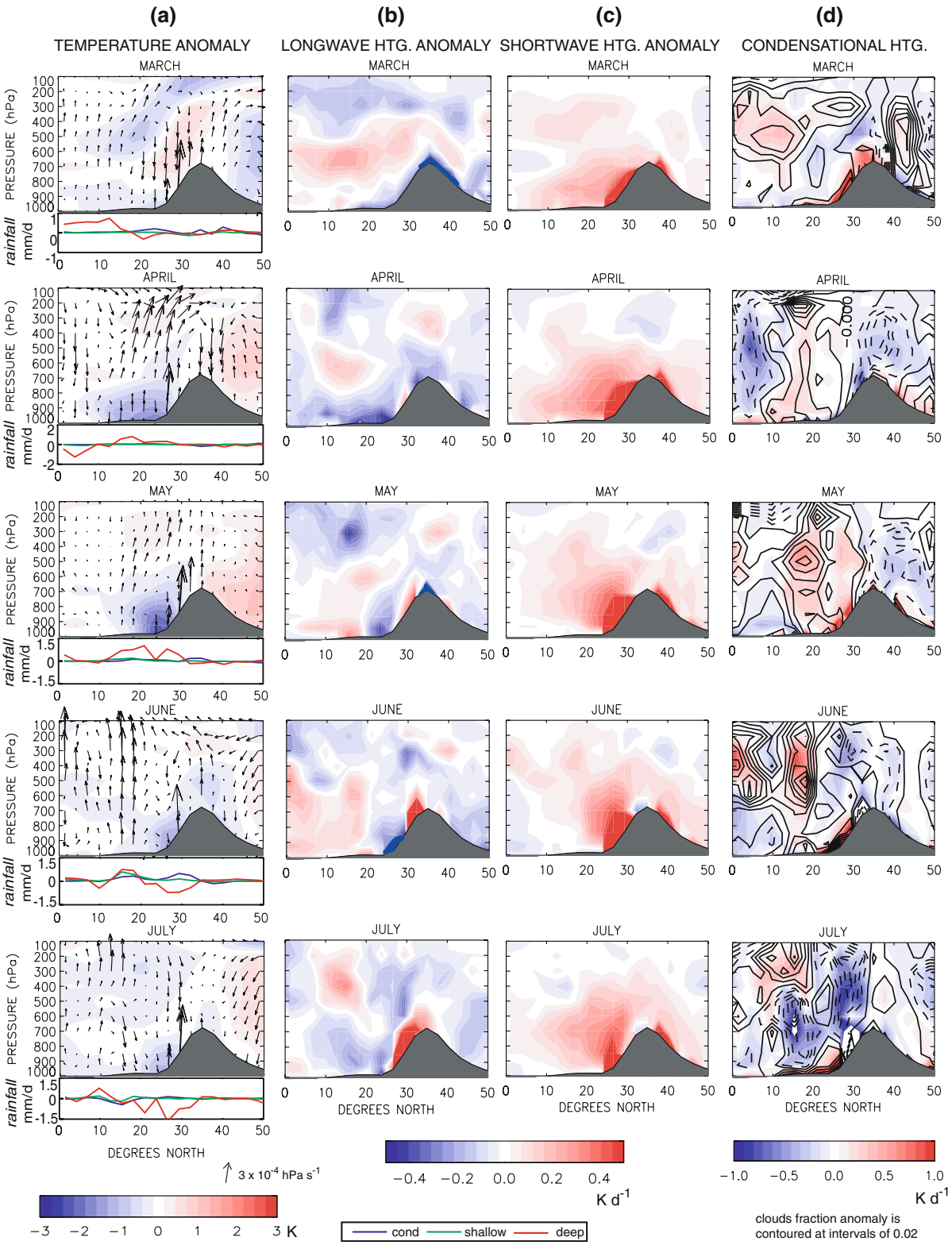

Fig. 7 Latitude-pressure plots of monthly-mean aerosol-induced anomalies of temperature, meridional circulation, and precipitation (**a**), longwave heating (**b**), shortwave heating (**c**), and condensational heating and cloud fraction (**d**) as averaged over the longitudes of 70–84°E for the ensemble of MATCH-forced CAM3 simulations

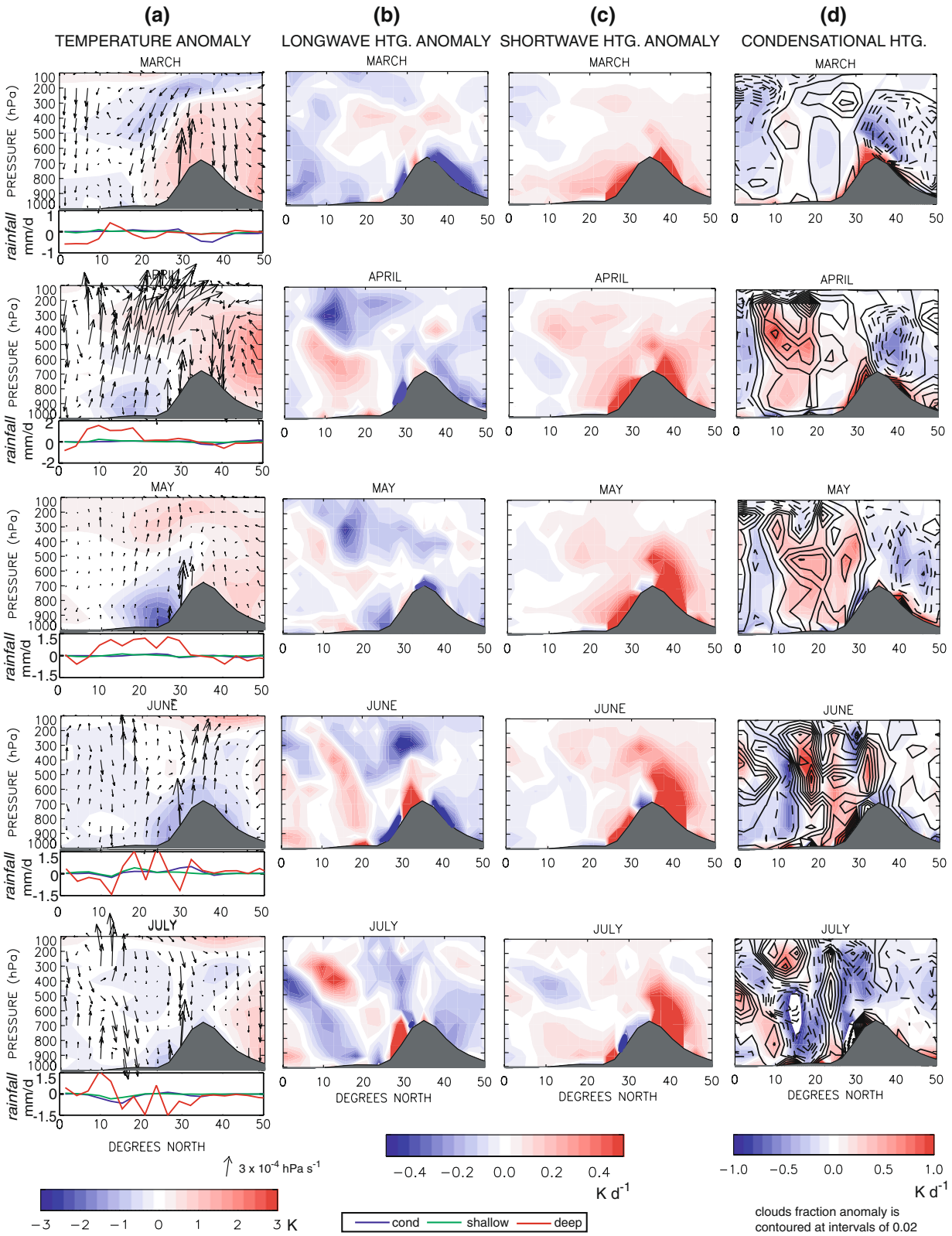

Fig. 8 Same as in Fig. 7 except for the GOCART-forced CAM3 simulations

et al. (2006) experiment, the stable air mass equatorward of the Himalayas is diminished. However, relative to the MATCH runs, the GOCART runs continue to show increased deep convective cloud between 20° and 30°N, giving rise to greater precipitation, particularly at 25°N. The reasons for this difference are not clear, but might be related to MATCH-GOCART shortwave heating differences on the southern slope. Increased heat in the MATCH runs may be mixing vertically to evaporate the convective cloud from below.

In July, the overall near-surface temperature anomaly is much reduced relative to previous months. However, longwave heating on the southern slope is significantly enhanced. This feature may be explained by the radiative effects of increased low cloud that has developed over the southern slope, indicative of a more stable atmosphere. It is possible that surface cooling in conjunction with aerosol-induced lower-tropospheric warming can enhance the formation of fog, an issue which has been raised by Satheesh et al. (2007). Consistent with the increased stability, monthly-mean precipitation from deep convection (and thus precipitation overall) is decreased relative to the no-aerosols simulations.

While increased atmospheric stability may play a significant role in the rainfall decrease, surface circulation anomalies also contribute in an important way. During July, and months prior, surface circulation over the Indian subcontinent is dominated by a trough of low pressure, around which southwesterly winds pick up moisture from the Arabian Sea and the Bay of Bengal and converge over India. This is a well-known response to temperature differences between land and sea (see Fig. 9a). However, as Fig. 9b, c reveals, both sets of aerosol-forced simulations are marked by higher than normal sea-level pressure over central India during May, an anomaly which expands geographically in June. By July, the sea-level pressure anomaly has become so large as to encompass the entire subcontinent and actually results in a weakened cyclonic circulation, as indicated by the anomalous anticyclonic flow, with a center over the northwestern Bay of Bengal.

It is interesting to see such a pronounced pressure anomaly over the ocean, given that the same monthly SST boundary conditions drive each simulation. Hydrostatic balance ensures that the only way such a rise in sea-level pressure can occur is if there is a drop in mean-column atmospheric temperature, but since SST is constrained to be fixed, the temperature anomaly must occur well-removed from the surface. Figure 10a shows the latitude-height temperature anomaly as averaged over the longitudes corresponding to the northwestern Bay of Bengal (80–90°E) and reveals that in general, for northwestern Bay of Bengal latitudes (10–20°N), there is net cooling between the surface and the tropopause (100–200 hPa). Since heating anomalies due to longwave and shortwave absorption (Fig. 10b, c) tend to cancel each other, reduced latent heating (Fig. 10d), through a deep column of the troposphere, accounts for the majority of this negative temperature anomaly. The large contribution from condensational heating reduction would be reasonable given a reduced flux of water vapor into the atmosphere. Maps of July-mean surface latent heat flux anomaly in Fig. 11 confirm that, in both sets of simulations, surface evaporation from the western and northwestern Bay of Bengal is reduced by as much as 30–40 W m^{-2} relative to the simulations with no aerosols. Given the fixed SST, this reduction must be accomplished by reduced surface wind speeds on the equatorward side of the cyclonic circulation. Refer back to Fig. 9, which shows that when compared to the no-aerosols simulations, the CAM3 (MATCH) and CAM3 (GOCART) circulations are characterized by weak westerlies over the Bay of Bengal during July. Thus, the anomalous low-level circulation induced by the presence of aerosols in the simulations not only reduces the transport of water vapor to the Indian subcontinent but, through its effect on the latent heat flux, it also diminishes the source of water vapor available for transport. One might speculate that if the SST were allowed to interact with the atmosphere, such as in a fully coupled configuration, the reduced near-surface winds would allow SST to increase, thus offsetting the reduction in surface latent heat flux realized in the uncoupled mode. In the present configuration, inclusion of aerosols leads to a weakening of the surface trough over the region and an anomalous anticyclonic circulation which represses the import of moisture for monsoonal precipitation during July.

The cause for such an anomalous circulation is linked to the vertically distributed aerosol-induced heating anomalies presented earlier. Refer to Figs. 12 and 13 which demonstrate the strong correlations between aerosol-induced anomalies of cloud fraction, surface temperature, mean tropospheric temperature (as weighted by the tropospheric depth), and sea-level pressure. Over land, convective cloud is increased due to the destabilizing effect of aerosol radiative absorption (column A). This increase in cloud reduces surface temperature (column B). Changes in surface temperature strongly affect mean tropospheric temperature (column C), as for most locations, the anomaly patterns of surface temperature and mean tropospheric temperature resemble each other. However, there are a few locations over land in which they do not. For these areas, upper-tropospheric heating/cooling is playing a large role. Recall from Figs. 7 and 8 that from April through May, there is diabatic heating aloft (due to both shortwave absorption

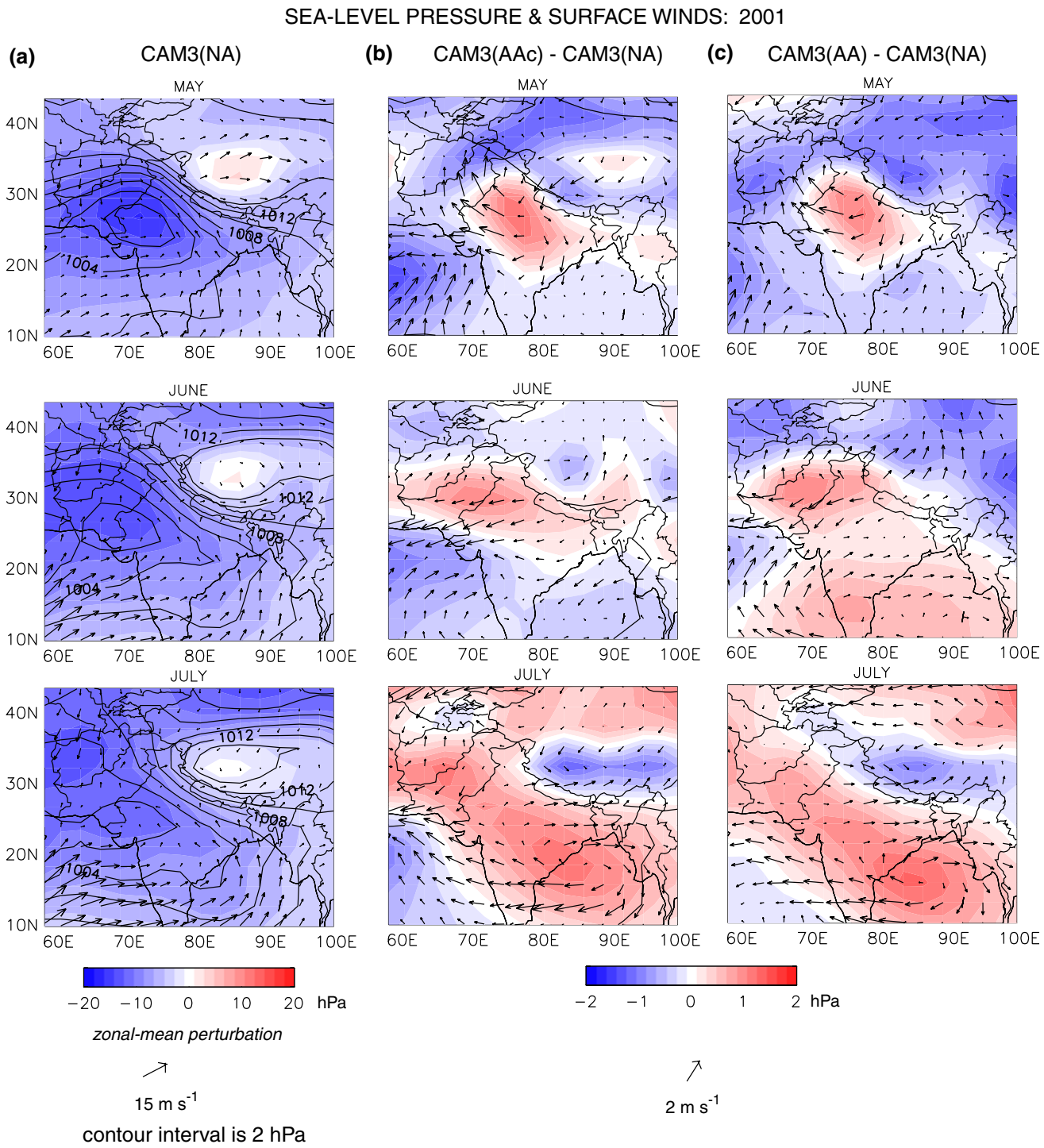

Fig. 9 Monthly-mean sea-level pressure in hPa (*contoured*), its zonal-mean perturbation (*shaded*), and surface winds for the CAM3 (NA) ensemble mean (**a**). Aerosol-induced anomalies are shown for CAM3(MATCH) (**a**) and CAM3 (GOCART) (**b**)

and condensation) but by June-July, upper tropospheric temperature anomalies diminish due to a reduction in both shortwave and latent heating. Over the ocean, surface temperature anomalies are zero, so mean tropospheric temperature anomalies here are dominated by middle and upper-tropospheric temperature changes. As shown in Fig. 10, the reduction of condensational heating during July causes net-column cooling over the

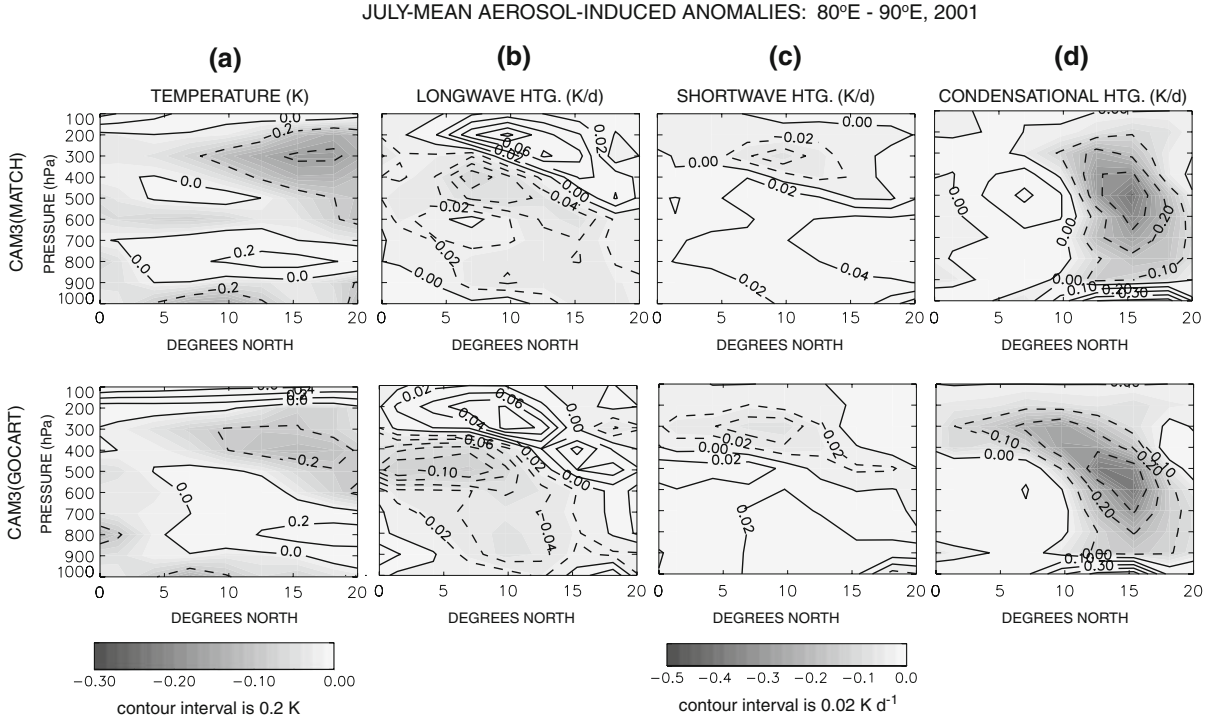

Fig. 10 July-mean aerosol-induced anomalies of temperature (K) (**a**), longwave heating (K/d) (**b**), shortwave heating (K/d) (**c**), and condensational heating (K/d) (**d**) for the MATCH- and GOCART-forced runs of CAM3. Note that only negative anomalies are shaded by intensity

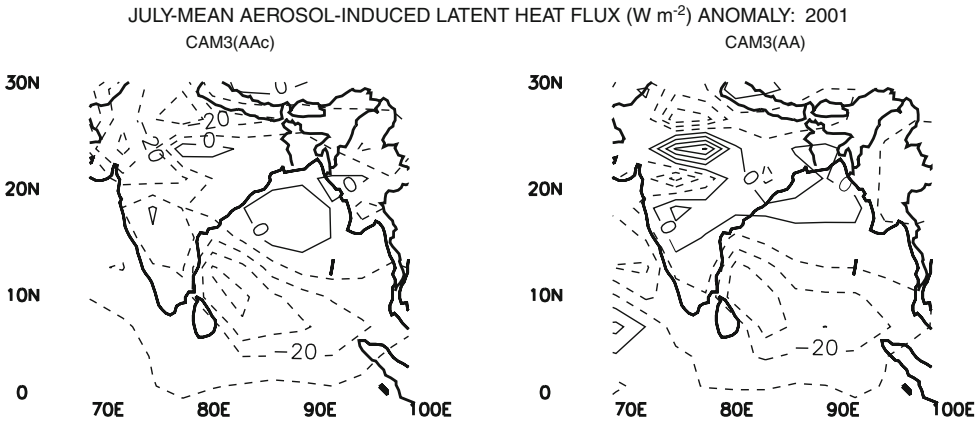

Fig. 11 July-mean aerosol-induced surface latent heat flux anomaly (W m^{-2}) for the MATCH- and GOCART-forced runs of CAM3. Note that a negative anomaly indicates a *reduced* flux of latent heat from the surface to the atmosphere. Contour interval is 10 W m^{-2}

Bay of Bengal. The hydrostatic response to the net cooling, over both the land and sea, is a higher sea-level pressure (column D), relative to simulations with no aerosols.[3]

[3] Assuming the tropopause is fixed at 200 hPa, then for a known surface geopotential, the natural log of sea level pressure is inversely proportional to the ratio of the mean tropospheric temperature to the geopotential thickness of the surface—200 hPa layer.

4 Summary and conclusions

The following conclusions may be drawn from this study.

1. Largest effects of aerosols on simulated surface climate over central India occur in May, when surface temperature is reduced by anywhere from 1 to 3 K and precipitation is increased by 1–2 mm day^{-1}. Enhanced atmospheric shortwave absorption due to the presence of black carbon and dust results in sensible and longwave heating of the underlying surface, though

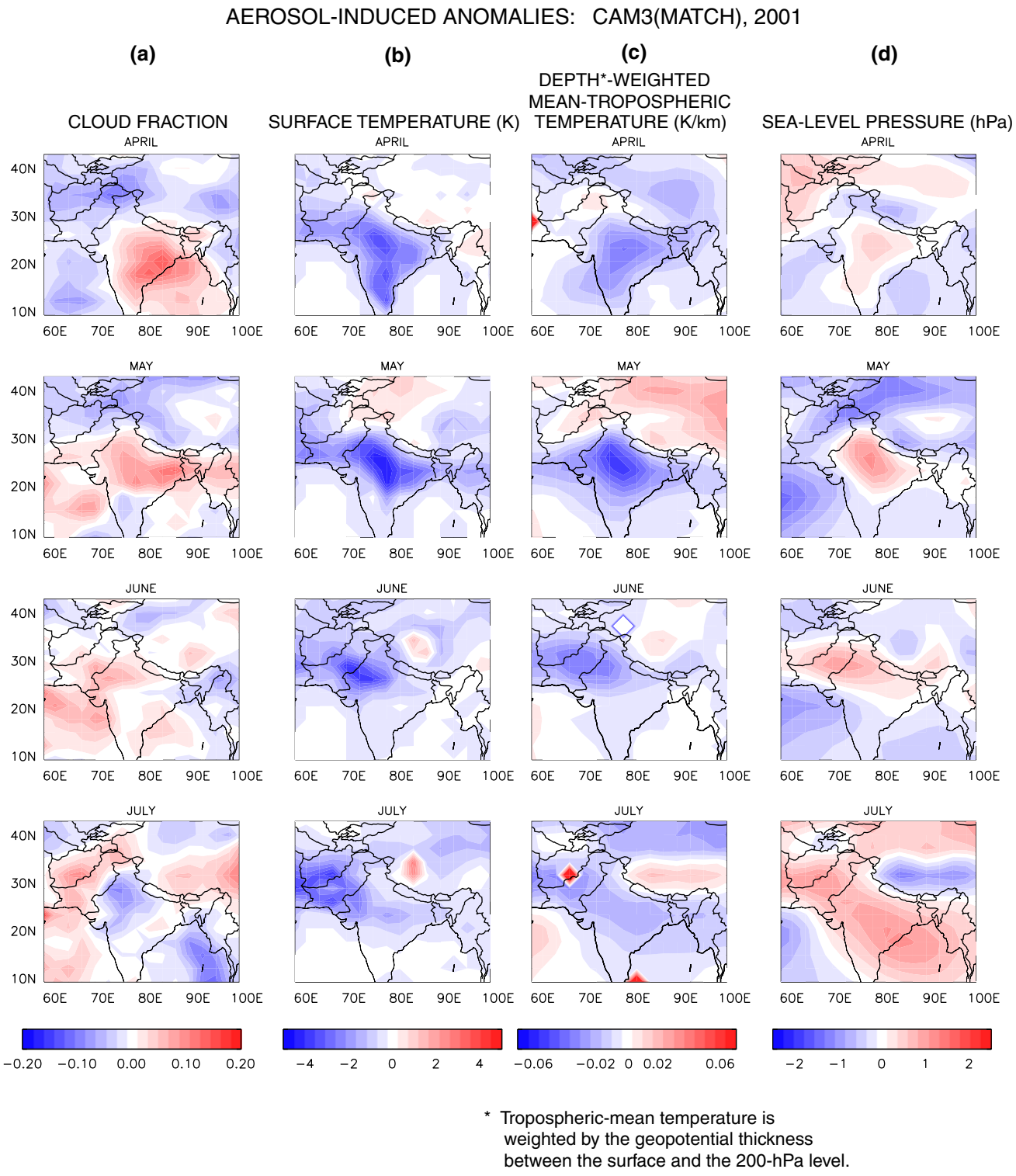

Fig. 12 April–July, 2001 aerosol-induced anomalies of cloud fraction (**a**), surface temperature in K (**b**), mean tropospheric temperature, as weighted by the tropospheric depth, in K/km (**c**), and sea-level pressure in hPa (**d**) for the CAM3 MATCH ensemble

these contributions are overwhelmed by reductions in surface shortwave and latent heatings which result in a net surface energy loss that continues into June.

2. The CAM3 monsoonal simulation is relatively insensitive to the differences between the three-dimensional aerosol distributions of the MATCH and GOCART

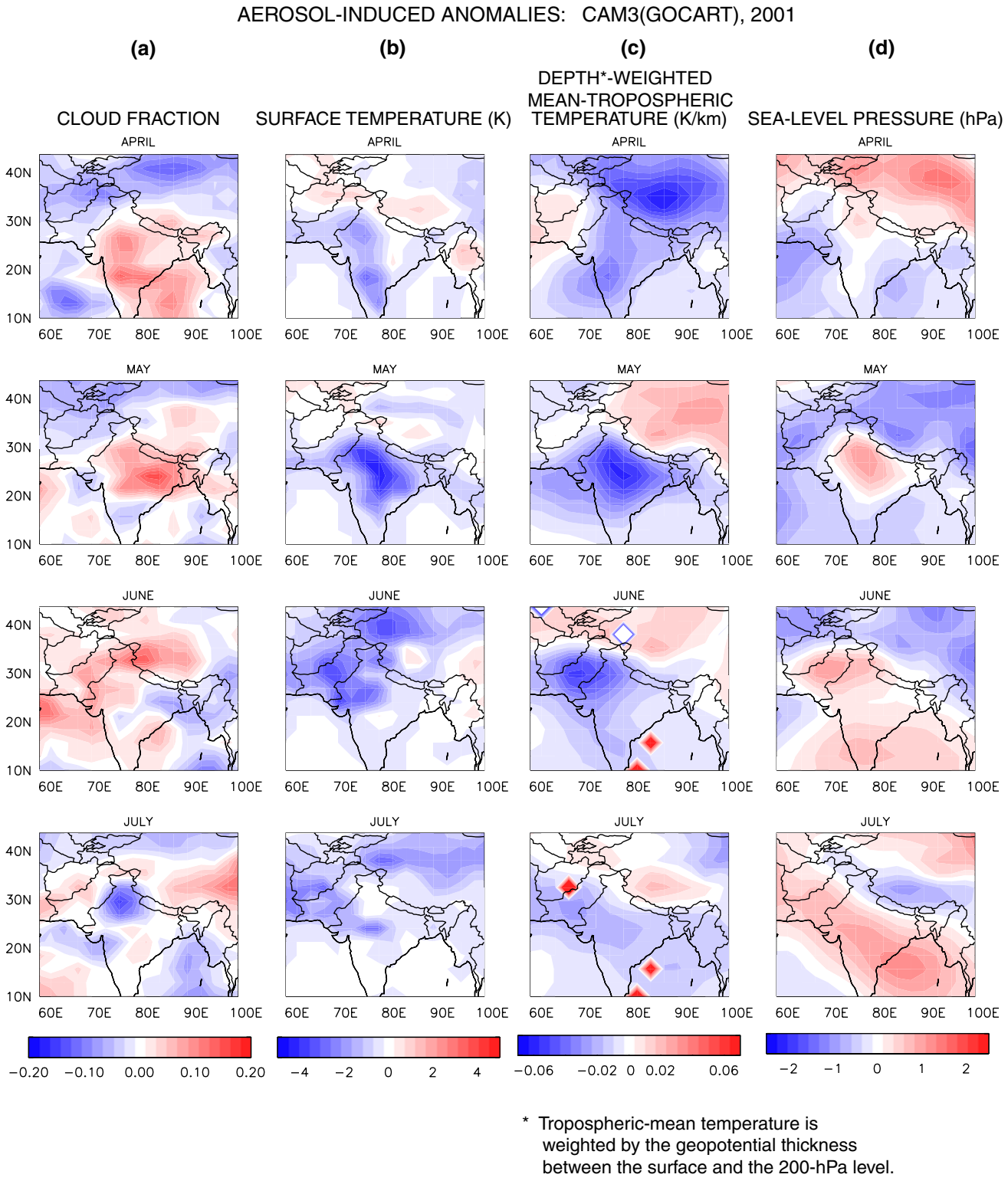

Fig. 13 Same as in Fig. 12 except for the CAM3 GOCART ensemble

products, though atmospheric shortwave heating differences are extreme over the northern slope of the Tibetan Plateau, where the masses of dust and black carbon differ most. Over central India, the presence of absorptive aerosols results in tropospheric shortwave heating on the order of 10–15% greater than that of simulations with no aerosol burden. This heating causes dry convection, which in turn draws in

warm moist air from the northern Indian Ocean to fuel cloud development and precipitation via the "elevated heat pump" mechanism of Lau et al. (2006); Lau and Kim (2006). The enhanced cloud reduces shortwave heating at the surface, which consequently, reduces the longwave heating of the overlying atmosphere. Additionally, increased evaporation due to the enhanced convective precipitation reduces surface latent heating.

3. The increased amount of water vapor, as drawn in from the south, condenses and contributes to heating the troposphere. The combination of enhanced latent and shortwave heating maintains a warm anomaly in the middle and upper troposphere, above the cool anomaly at and just above the surface. However, the cooling of the lower troposphere, due to reduced longwave emission and vertical heat diffusion from the surface, dominates the mean tropospheric column temperature anomaly, resulting in higher than normal sea level pressure over central India, relative to simulations with no aerosols.
4. In July, weakened surface wind speeds on the equatorward side of an aerosol-induced anomalous anticyclonic circulation reduce the latent heat flux from the ocean, thereby reducing upper-tropospheric condensational heating over the Bay of Bengal. This perpetuates the anomalously high sea level pressure and anticyclonic anomaly that serves to reduce the availability of moisture to India, resulting in diminished precipitation relative to the previous month and relative to simulations with no aerosols. Therefore, it is proposed that while absorptive aerosols enhance simulated tropospheric shortwave heating to induce dry convection and draw in moisture from the south for monsoon strengthening, the enhanced precipitation and cloud cover cool the surface, and thus the lower troposphere, too severely, creating a negative feedback. Mean tropospheric cooling weakens the surface monsoon trough, which acts to decrease moisture supply from the ocean causing a reduction in monsoon rainfall. It should be caveated, however, that this effect is purely dynamical resulting from the initial anomalies set up by aerosol loading, and highly variable from model to model.

In summarizing the important results presented in this study, it is useful to consider some of this experiment's limitations. First, in the CAM3 simulations, aerosols cannot interact with the model, but must be prescribed. Therefore, scavenging, diffusion, and transport of aerosols, which have the potential to alter horizontal and vertical distributions, and thus anomalous heating rates, are neglected processes, though they are accounted for in the GOCART model itself (Ginoux et al. 2001). Similarly, the model cannot allow for aerosols to act as cloud condensation nuclei, thereby enhancing cloud reflectivity [the first indirect effect (Twomey 1974)] and/or alter cloud precipitation efficiency [the second indirect effect (Albrecht 1989; Pincus and Baker 1994)]. This limitation is typical of general circulation models, whose length scales are generally too large to resolve cloud-aerosol interactions, though these effects can be measured by coupling online aerosol models to GCMs [e.g., (Menon et al. 2002a)]. In recent years, explicit parameterizations of the indirect effect have been proposed and tested (Nenes and Seinfeld 2003; Lohmann and Diehl 2006). A second constraint on the experiment is that in the CAM3, aerosols cannot be internally mixed. That is, a single particle cannot be composed of two different species. A particle consisting of both sulfate and soot, for example, may have entirely different optical properties than one consisting of either species alone. This limitation is shared with the experiment of Lau et al. (2006). While the above limitations cannot be lifted without altering the model itself, there are others which were optional. First, while the use of multiple statistically independent simulations allowed estimation of a range of uncertainty on aerosol-induced anomalies, simulations carried out spanned the course of only one year. Thus, the aerosol-induced anomalies measured, while representative of the model for 2001, may not be representative of any given year, though observations from the Xie–Arkin data indicate that the annual cycle of precipitation over central India for 2001 is qualitatively similar to those for the previous 10 years. The extension of these model runs or a repeat of these simulations using a climatological SST boundary condition is needed for assessing the robustness of the features observed. However, both sets of simulations would require a longer record of data from the GOCART model. Secondly, SST is not forced by the atmospheric simulation. While the aim of the current study was to measure sensitivity of the atmospheric simulation to aerosol loading, results suggest that a similar sensitivity study with the fully coupled version of the model may yield interesting results, particularly given the importance of the Indian Ocean and the Bay of Bengal in particular for moisture availability to the monsoon. It is evident from these simulations that aerosol shortwave heating has at least an indirect effect on the latent heat flux from the adjacent ocean waters via the mean near-surface circulation.

Acknowledgments This research was supported by the U.S. National Science Foundation grant ATM-0601781 and by the Biological and Environmental Research Program (BER), US Department of Energy under grant DE-FG02-03ER63532. The authors thank the reviewers for their constructive comments that have helped improve the presentation of the paper.

References

Albrecht B (1989) Aerosols, cloud microphysics, and fractional cloudiness. Science 245(4923):1227

Andreae M (2001) The dark side of aerosols. Nature 409(6821):671–672

Babu SS, Moorthy KK, Satheesh S (2004) Aerosol black carbon over Arabian Sea during intermonsoon and summer monsoon season. Geophys Res Lett 31(L06104). doi:10.1029/2003GL018716

Boucher O, Anderson T (1995) General circulation model assessment of the sensitivity of direct climate forcing by anthropogenic sulfate aerosols to aerosol size and chemistry. J Geophys Res 100(D12):26117–26134

Braslau N, Dave J (1975) Atmospheric heating rates due to solar radiation for several aerosol-laden cloudy and cloud-free models. J Appl Meteor 14:396–399

Charlock TP, Sellers WD (1980) Aerosol effects on climate: calculations with time-dependent and steady-state radiative–convective models. J Atmos Sci 37:1327–1341

Charlson RJ, Schwartz S, Hales J, Cess R, JA Coakley J, Hansen J, Hofmann D (1992) Climate forcing by anthropogenic aerosols. Science 255(5043):423–430

Chin M, Ginoux P, Kinne S, Torres O, HOlben BN, Duncan BN, Martin RV, Logan JA, Higurashi A, Nakajima T (2002) Tropospheric aersosol optical thickness from the GOCART model and comparisons with satellite and sun photometer measurements. J Atmos Sci 59:461–483

Chung CE, Zhang GJ (2004) Impact of absorbing aerosol on precipitation: dynamic aspects in association with convective available potential energy and convective parameterization closure and dependence on aerosol heating profile. J Geophys Res 109(D22103). doi:10.1029/2004JD004726

Collins W et al (2006) The community climate system model version 3 (CCSM3). J Clim 19:2122–2143

Collins W, Rasch P, Boville B, Hack J, McCaa J, Williamson D, Kiehl J, Briegleb B, Bitz C, Lin SJ, Zhang M, Dai Y (2004) Description of the NCAR community atmosphere model (CAM 3.0). NCAR technical note NCAR/TN-464+STR

Collins WD, Rasch PJ, Eaton BE, Fillmore DW, Kiehl JT (2002) Simulation of aerosol distributions and radiative forcing for INDOEX: regional climate impacts. J Geophys Res 107(D19, 8028). doi:10.1029/2000JD000032

Corrigan C, Ramanathan V, Schauer J (2006) Impact of monsoon transitions on the physical and optical properties of aersols. J Geophys Res 111(D18208). doi:10.1029/2005JD006370

Dickinson R, Oleson K, Bonan G, Hoffman F, Thornton P, Vertenstein M, Yang ZL, Zeng X (2006) The community land model and its climate statistics as a component of the community climate system model. J Clim 19:2302–2324

Ginoux P, Chin M, Tegen I, Prospero J, Holben B, Dubovik O, Lin S (2001) Sources and distributions of dust aerosols simulated with the GOCART model. J Geophys Res 106(D17):20255–20274

Hess M, Koepke P, Schult I (1998) Optical properties of aerosols and clouds: the software package opac. Bull Am Meteorol Soc 79:831–844

Kiehl J, Briegleb B (1993) The relative roles of sulfate aerosols and greenhouse gases in climate forcing. Science 260(5106):311

Kim J, Gu Y, Liou K (2006) The impact of direct aerosol radiative forcing on surface insolation and spring snowmelt in the Southern Sierra Nevada. J Hydrometeorol 7(5):976–983

Kristjansson J, Iversen T, Kirkevag A, Seland O (2005) Response of the climate system to aerosol direct and indirect forcing: role of cloud feedbacks. J Geophys Res 110(D24206). doi:10.1029/2005JD006299

Lau K, Kim M, Kim K (2006) Asian summer monsoon anomalies induced by aerosol direct forcing: the role of the Tibetan Plateau. Clim Dynam. doi:10.1007/s00382-006-0114-z:855-864

Lau KM, Kim KM (2006) Observational relationships between aerosol and Asian monsoon rainfall, and circulation. Geophys Res Lett 33(L21810). doi:10.1029/2006GL027546

Lelieveld J, Crutzen P, Ramanathan V, Andreae M, Brenninkmeijer C, Campos T, Cass G, Dickerson R, Fischer H, de Gouw J et al (1993) The Indian Ocean experiment: widespread air pollution from South and Southeast Asia. Science 259:71

Li F, Ramanathan V (2002) Winter to summer monsoon variation of aerosol optical depth over the tropical Indian Ocean. J Geophys Res 107(D16,4284). doi:10.1029/2001JD000949

Liao H, Seinfeld JH (1998) Effect of clouds on direct aerosol radiative forcing of climate. J Geophys Res 103(D4):3781–3788

Lohmann U, Diehl K (2006) Sensitivity studies of the importance of dust ice nuclei for the indirect aerosol effect on stratiform mixed-phase clouds. J Atmos Sci 63(3):968–982

Meehl GA, Arblaster JM, Collins WD (2008) Effects of black carbon aerosols on the Indian monsoon. J Clim (in press)

Menon S, Genio A, Koch D, Tselioudis G (2002a) GCM simulations of the aerosol indirect effect: sensitivity to cloud parameterization and aerosol burden. J Atmos Sci 59(3):692–713

Menon S, Hansen J, Nazarenko L, Luo Y (2002b) Climate effects of black carbon aerosols in China and India. Science 297(5590). doi:10.1126/science.1075159:2250-2253

Moorthy KK, Babu SS, Satheesh S, Srinivasan J, Dutt C (2007) Dust absorption over the "Great Indian Desert", inferred using ground-based and satellite remote sensing. J Geophys Res 112(D09206). doi:10.1029/2006JD007690

Moorthy KK, Babu SS, Satheesh SK (2005) Aerosol characteristics and radiative impacts over the Arabian Sea during the inter-monsoon season: results from ARMEX field campaign. J Atmos Sci 62:192–206

Nemesure S, Wagener R, Schwartz SE (1995) Direct shortwave forcing of climate by the anthropogenic sulfate aerosol: sensitivity to particle size, composition, and relative humidity. J Geophys Res 100(D12):26105–26116

Nenes A, Seinfeld J (2003) Parameterization of cloud droplet formation in global climate models. J Geophys Res 108:4415

Neumann J, Cohen A (1972) Climatic effects of aerosol layers in relation to solar radiation. J Appl Meteor 11:651–657

Oleson K, coauthors (2004) Technical description of the Community Land Model (clm). Technical report NCAR/TN-461+STR, NCAR, available from National Center for Atmospheric Research, Boulder, CO 80307

Pincus R, Baker M (1994) Effect of precipitation on the albedo susceptibility of clouds in the marine boundary layer. Nature 372(6503):250–252

Ramana M, Ramanathan V (2006) Abrupt transition from natural to anthropogenic aerosol radiative forcing: observations at the ABC-Maldives climate observatory. J Geophys Res 111(D20207). doi:10.1029/2006JD007063

Ramanathan V, Crutzen P, Kiehl J, Rosenfeld D (2001a) Aerosols, climate, and the hydrological cycle. Science 294(5549):2119–2124

Ramanathan V, Crutzen P, Lelieveld J, MItra A, Althausen D, Anderson J, Andreae M, Cantrell W, Cass G, Chung C, Clarke A, Coakley J, Collins W, Conant W, Dulac F, Heintzenberg J, Heymsfield A, Holben B, Howell S, Hudson J, Jayaraman A, Kiehl J, Krishnamurti TN, Lubin D, McFarquhar G, Novakov T, Ogren J, Podgorny I, Prather K, Priestley K, Prospero J, Quinn P, Rajeev K, Rasch P, Rupert S, Sadourny R, Satheesh S, Shaw G, Sheridan P, Valero F (2001b) Indian ocean experiment: an integrated analysis of the climate forcing and

effects of the great Indo-Asian haze. J Geophys Res 106(D22): 28371–28398

Satheesh SK, Dutt CBS, Srinivasan J, Rao UR (2007) Atmospheric warming due to dust absorption over Afro-Asian regions. Geophys Res Lett 34:L04805. doi:10.1029/2006GL028623

Satheesh S, Srinivasan J (2002) Enhanced aerosol loading over Arabian Sea during the pre-monsoon season: natural or anthropogenic? Geophys Res Lett 29(18):21–1

Takemura T, Nakajima T, Dubovik O, Holben BN, Kinne S (2002) Single-scattering albedo and radiative forcing of various aerosol species with a global three-dimensional model. J Clim 15(4):333–352

Takemura T, Nozawa T, Emori S, Nakajima TY, Nakajima T (2005) Simulation of climate response to aerosol direct and indirect effects with aerosol transport-radiation model. J Geophys Res 110(D02202). doi:10.1029/2004JD005029

Taylor KE, Williamson D, Zwiers F (2000) The sea surface temperature and sea-ice concentration boundary conditions for AMIP II simulations. Technical report 60, Program for Climate Model Diagnosis and Intercomparison, Lawrence Livermore National Laboratory

Twomey S (1974) Pollution and the planetary albedo. Atmos Environ 8:1251–1256

Zender C, Bian H, Newman D (2003) The mineral dust entrainment and deposition (dead) model: description and 1990s dust climatology. J Geophys Res 108

Zhang G, McFarlane NA (1995) Sensitivity of climate simulations to the parameterization of cumulus convection in the Canadian Climate Centre general circulation model. Atmos Ocean 33:407–446